Electrochimica Acta 555 (2026) 148402

Contents lists available at ScienceDirect

Electrochimica Acta

journal homepage: www.journals.elsevier.com/electrochimica-acta

Recursive RC Modeling for Time-Domain Estimation of the Distribution of Relaxation Times

Marvin Malchau *, Jan Philipp Schmidt

University of Bayreuth, Bavarian Center for Battery Technology (BayBatt), Chair of Systems Engineering for Electrical Energy Storage (SysEE), Universitätsstraße 30, 95447 Bayreuth, Germany

ARTICLE INFO

Keywords:
Lithium-Ion
DRT
EIS
Time-Domain
Modeling

ABSTRACT

We propose a time-domain method for estimating the Distribution of Relaxation Times (DRT) in electrochemical systems based on a recursive RC modeling framework. By discretizing the system response via bilinear transformation, this approach enables direct reconstruction of the DRT from arbitrary current excitation signals, without relying on frequency-domain impedance data or predefined excitation profiles, as required by established methods such as pulse-fitting. The method integrates multiple electrochemical contributions into a unified linear model and solves the resulting inverse problem using nonnegative least squares with Tikhonov regularization. Validation with synthetic and experimental data demonstrates high accuracy, numerical stability, and excellent agreement with conventional impedance spectroscopy. The approach significantly reduces measurement time, especially in the low-frequency regime, and offers robust performance under realistic noise conditions.

1. Introduction

The continuously increasing demand for advanced electrical energy storage systems has not only driven innovation in battery design and performance but has also intensified the need for precise and efficient diagnostic tools in both research and practical applications. Among the available diagnostic techniques, electrochemical impedance spectroscopy (EIS) has long been established as a standard method for lithium-ion cell analysis due to its unique capability to characterize the complex frequency response of electrochemical systems. In a typical EIS measurement, single or multiple sinusoidal excitation signals are applied to the cell, and the resulting impedance is determined across a wide frequency range. This frequency-domain representation provides valuable insights into internal kinetics and transport processes, typically visualized using Nyquist or Bode plots. While these graphical representations facilitate the interpretation of underlying electrochemical phenomena, they are not particularly.[1,2]

Furthermore, the instrumentation required for EIS is both complex and expensive, as it necessitates precise signal generation and high-fidelity measurement electronics. In addition, EIS is subject to several inherent limitations. At low frequencies, the duration of the excitation signal increases substantially, leading to prohibitively long measurement times. During these extended measurements, charge accumulation over half-cycles can alter the cell's state of charge, thereby violating the quasi-stationary assumption essential for accurate impedance determination.

While Nyquist and Bode plots provide a direct visualization of the impedance spectrum, their interpretation often requires considerable expertise due to overlapping relaxation processes and non-ideal system behavior. A major challenge arises from the fact that contributions from slower processes accumulate at lower frequencies, making it difficult to disentangle individual effects. In contrast, the Distribution of Relaxation Times (DRT) offers a more intuitive and physically meaningful representation by directly mapping the underlying processes to their characteristic time constants [3]. The DRT is formally related to the impedance $Z(\omega)$ through the integral

$$Z(\omega) = R_\infty + \int_{-\infty}^{\infty} \frac{\gamma(\tau)}{1 + j\omega\tau}\, d\ln\tau, \tag{1}$$

where $\gamma(\tau)$ denotes the distribution function representing the polarization resistances associated with different electrochemical processes, τ is the characteristic time constant, and R_∞ represents the high-frequency ohmic resistance. This formulation enables the deconvolution of complex impedance spectra into a distribution of relaxation times.

Estimating the Distribution of Relaxation Times (DRT) from experimental impedance spectra is a well-known ill-posed inverse problem. The solution is highly sensitive to measurement noise and often suffers from non-uniqueness and instability. Regularization techniques, such as Tikhonov regularization [4], are commonly used to stabilize the

* Corresponding author.
E-mail address: marvin.malchau@uni-bayreuth.com (M. Malchau).

https://doi.org/10.1016/j.electacta.2026.148402
Received 2 December 2025; Received in revised form 14 January 2026; Accepted 6 February 2026
Available online 10 February 2026

solution, but their effectiveness depends critically on the choice of regularization parameters and may introduce systematic bias if not properly tuned.

To address the limitations of frequency-domain methods and reduce the complexity of measurement instrumentation, time-domain approaches have gained increasing attention. These methods offer a more accessible and often more intuitive alternative, particularly in systems where high-resolution impedance data is difficult to obtain or interpret. One common strategy involves fitting voltage transients with sums of exponential functions to extract relaxation time constants and amplitudes directly [5,6]. While conceptually appealing, this method is highly sensitive to noise and excitation characteristics, often resulting in unstable or biased estimates. Another approach fits equivalent circuit models (ECMs) to time-domain data. These models represent the system as a set of discrete relaxation processes, effectively yielding a discretized DRT [7]. However, ECMs rely on prior assumptions about the system structure and may fail to capture overlapping or complex dynamics. Model-free techniques such as Fourier [8], Laplace [9], or wavelet transformations [10] convert time-domain signals into impedance spectra. Fourier-based methods are prone to spectral leakage due to finite observation windows and non-periodic signal boundaries, which can lead to scattering and distortion in the impedance spectrum. In contrast, Laplace and wavelet transforms are not susceptible to classical spectral leakage, although wavelet-based methods may still introduce artifacts depending on the choice of basis and noise conditions. These distortions can manifest as scattering and outliers in the impedance spectrum and complicate subsequent DRT reconstruction, which again requires solving the ill-posed inverse problem defined in Eq. (1).

Since its introduction, the DRT has been applied in a variety of contexts. Kasper et al. [11] used a time-domain approach to reconstruct electrochemical impedance spectra from current pulses, modeling the cell as discrete RC elements implemented as a digital IIR filter via bilinear transformation, assuming constant sampling intervals. DRT weights are obtained through least-squares fitting. While this method effectively links time- and frequency-domain representations, it is not directly suited for experimental data with non-uniform time steps. Beyond this, the DRT is widely used, for example, to extract the main contributing time constants and their weights, to find initial values for equivalent circuit models [12] for battery modeling or state estimation [13], to analyze cell-to-cell variations [14], aging and degradation [15–17] or to capture slow relaxation processes and hysteresis in LFP cells for improved SoC estimation [18].

In this work, we present a time-domain framework for DRT estimation based on recursive RC modeling. Our method discretizes the continuous-time RC network using a bilinear transformation and formulates the system response as a linear combination of recursive kernels. The resulting inverse problem is solved using nonnegative least squares with Tikhonov regularization, ensuring numerical stability and physical interpretability. Unlike previous approaches, our method enables direct DRT reconstruction from arbitrary current excitation signals without relying on frequency-domain data or predefined circuit models. It supports flexible excitation designs, reduces measurement time — particularly in the low-frequency regime — and demonstrates robust performance under realistic noise conditions. Theoretical foundations and validation through simulation and experimental data confirm the method's accuracy, adaptability, and computational efficiency, offering a promising pathway for reliable DRT analysis in complex electrochemical systems.

2. Method

In this section, we detail the theoretical foundation of our proposed time-domain DRT estimation method. We begin with a basic RC element, derive its governing equations, and then extend the derivation using standard transformation techniques. The approach presented here is well supported in the literature [19,20].

2.1. Continuous-time differential equation

For a simple parallel RC element, Kirchhoff's current law states that the total current flowing into the node is given by the sum of the currents through the resistor and the capacitor. Mathematically, we have:

$$I(t) = I_R(t) + I_C(t), \tag{2}$$

where the resistor current is defined as

$$I_R(t) = \frac{U(t)}{R}, \tag{3}$$

and the capacitor current is expressed by the capacitor's constitutive relation:

$$I_C(t) = C\,\frac{dU(t)}{dt}. \tag{4}$$

Substituting Eqs. (3) and (4) into (2) yields:

$$I(t) = \frac{U(t)}{R} + C\,\frac{dU(t)}{dt}. \tag{5}$$

Multiplying both sides of (5) by R and defining the time constant $\tau = RC$, we obtain:

$$\tau\,\frac{dU(t)}{dt} + U(t) = R\,I(t). \tag{6}$$

This differential equation forms the basis for analyzing the RC network in the time domain.

2.2. Laplace domain representation

To facilitate the solution of the differential equation, we apply the Laplace transform. Assuming zero initial conditions, $U(0) = 0$, the Laplace transform of Eq. (6) gives:

$$\tau\,s\,U(s) + U(s) = R\,I(s). \tag{7}$$

Here, $U(s)$ and $I(s)$ are the Laplace transforms of $U(t)$ and $I(t)$, respectively. Factoring $U(s)$ from the left-hand side results in:

$$U(s)\,(\tau s + 1) = R\,I(s). \tag{8}$$

Thus, the transfer function $H(s)$ of the RC element is given by:

$$H(s) = \frac{U(s)}{I(s)} = \frac{R}{\tau s + 1}. \tag{9}$$

This representation is standard in linear system theory [19].

2.3. Bilinear transformation

To implement the model in discrete time, we need to convert the continuous-time transfer function $H(s)$ into the z-domain. We achieve this by applying Tustin's bilinear transform, which is defined as:

$$s = \frac{2}{T}\,\frac{1 - z^{-1}}{1 + z^{-1}}, \tag{10}$$

where T is the sampling period. Substituting (10) into the transfer function in (9):

$$H(z) = \frac{R}{\tau\left(\frac{2}{T}\,\frac{1-z^{-1}}{1+z^{-1}}\right) + 1}.$$

Multiplying the numerator and the denominator by $(1+z^{-1})$ to simplify, we arrive at the following.

$$H(z) = \frac{R\,(1 + z^{-1})}{\left(1 + \frac{2\tau}{T}\right) + \left(1 - \frac{2\tau}{T}\right) z^{-1}}. \tag{11}$$

For convenience, we define:

$$a = \frac{2\tau}{T}. \tag{12}$$

Thus, Eq. (11) is rewritten as:

$$H(z) = \frac{R\,(1 + z^{-1})}{(1 + a) + (1 - a)z^{-1}}. \tag{13}$$

This transformation preserves the frequency response over the interval of interest and is widely used in digital signal processing [20].

2.4. Recursive formulation in time

To interpret the discrete-time transfer function $H(z)$ in the time domain, we recognize that it represents the ratio $U(z)/I(z)$. Rearranging (13) by cross-multiplying yields:

$$(1 + a)\,U(z) + (1 - a)\,z^{-1}U(z) = R\,(1 + z^{-1})I(z). \tag{14}$$

Taking the inverse z-transform and noting that multiplication by z^{-1} corresponds to a delay of one sample, we obtain the following discrete-time recursion:

$$(1 + a)\,u(n) + (1 - a)\,u(n - 1) = R\,[\,I(n) + I(n - 1)\,]. \tag{15}$$

Solving Eq. (15) for $u(n)$ leads to:

$$u(n) = \alpha\,[\,I(n) + I(n - 1)\,] \;-\; \beta\,u(n - 1), \tag{16}$$

with the coefficients defined as:

$$\alpha = \frac{R}{1 + a}, \quad \beta = \frac{1 - a}{1 + a}. \tag{17}$$

This recursion forms the basis of our RC kernel approximation. It allows the decomposition of the continuous-time RC response into a sequence of discrete updates, suitable for rapid simulation and estimation in time-domain DRT analysis.

2.5. Extended model structure

Now, we elaborate on our approach for estimating the DRT by extending the analysis from a single RC element to an ensemble of RC elements. Our model integrates a series resistance R_0, an offset voltage U_0, and the differential capacity C_{diff} to comprehensively describe the behavior of the battery system. The following subsections describe the various steps in our methodology.

Our model expresses the measured voltage $U(t)$ as a sum of contributions from different electrochemical processes:

$$U(t) = R_0\,I(t) \;+\; U_0 \;+\; \sum_{i=1}^{N_{\text{DRT}}} R_i\,K_i(t) + \frac{1}{C_{\text{diff}}}\int_0^t I(\tau)\,d\tau, \tag{18}$$

where each $K_i(t)$ is the discrete-time response of an RC element associated with a characteristic time constant τ_i. The summation term aggregates the effects of N_{DRT} relaxation processes.

2.6. Recursive kernels and integration term

Each individual kernel $K_i(t)$ is calculated recursively. The recursion is based on the discretized version of the RC network response—similar to the formulation given in Eq. (16) for the single RC element. For each process i, the recursive update is:

$$K_i(n) = \alpha_i\,[I(n) + I(n - 1)] \;-\; \beta_i\,K_i(n - 1), \tag{19}$$

with coefficients $\alpha_i = \frac{1}{1+a_i}$ and $\beta_i = \frac{1-a_i}{1+a_i}$ where $a_i = \frac{2\tau_i}{T}$. This discrete-time formulation permits fast numerical simulation and is analogous to methods found in digital signal processing textbooks [19,20].

The differential capacity term is represented by an integration of the current signal $I(t)$. We use a trapezoidal rule to approximate the integral:

$$K_C(n + 1) = K_C(n) + \frac{1}{2}\,[I(n) + I(n + 1)]\,\Delta t_n, \tag{20}$$

which approximates $\int_0^{t(n)} I(\tau)\,d\tau$. Such numerical integration techniques are well documented in literature on numerical methods [21].

2.7. Design matrix formulation

To incorporate all model components into a unified estimation framework, we construct a design matrix $\mathbf{A}$ that consolidates the contribution of the RC kernels, the integrated current, the raw current, and a bias term. Mathematically, $\mathbf{A}$ is formulated as:

$$\mathbf{A} = \begin{pmatrix} | & \cdots & | & | & | & | \\ \mathbf{K}_1 & \cdots & \mathbf{K}_{N_{\text{DRT}}} & \mathbf{K}_C & \mathbf{I} & \mathbf{1} \\ | & \cdots & | & | & | & | \end{pmatrix}, \tag{21}$$

where $\mathbf{K}_1, \ldots, \mathbf{K}_{N_{\text{DRT}}}$ are the column vectors of the individual RC kernels sampled over time, $\mathbf{K}_C$ is the integrated current term (related to C_{diff}), $\mathbf{I}$ represents the measured current, and $\mathbf{1}$ is a column of ones corresponding to the offset U_0.

The unknown parameter vector is defined as:

$$\mathbf{x} = \left(R_1, \ldots, R_{N_{\text{DRT}}},\ \frac{1}{C_{\text{diff}}},\ R_0,\ U_0\right)^T. \tag{22}$$

The design matrix relates the model parameters to the measured voltage vector $\mathbf{U}$ as:

$$\mathbf{U} \approx \mathbf{A}\,\mathbf{x}. \tag{23}$$

This matrix formulation is a standard approach in system identification and linear inverse problems [22,23].

2.8. Tikhonov regularization

Since the estimation of $\mathbf{x}$ from $\mathbf{U}$ is an ill-posed problem, regularization is necessary to obtain stable and physically plausible solutions. We employ Tikhonov regularization by introducing a second-difference operator $\mathbf{D}$ to impose smoothness on the estimated DRT spectrum. The augmented minimization problem is:

$$\min_{\mathbf{x}\geq 0}\ \|\mathbf{A}\,\mathbf{x} - \mathbf{U}\|_2^2 + \lambda^2\,\|\mathbf{D}_{\text{aug}}\,\mathbf{x}\|_2^2, \tag{24}$$

where λ is the regularization parameter and $\mathbf{D}_{\text{aug}}$ is the block-augmented difference operator that acts on the parameters corresponding to the DRT. Tikhonov regularization is widely used for stabilizing the solution of ill-posed inverse problems, as discussed in detail in [22]. To determine a suitable value for the regularization parameter, several methods have been proposed in the literature, such as cross-validation and the L-curve method [24]. Although these approaches are well established, their applicability to time-domain methods remains to be evaluated.

2.9. Nonnegative Least Squares (NNLS)

A non-negativity constraint is imposed on the DRT in order to obtain a directly physically interpretable distribution of resistive relaxation processes. This constraint restricts the applicability of the method to linear, time-invariant, and dissipative systems, which is consistent with the assumptions underlying the RC-based DRT formulation used in this work.

$$\mathbf{x} = \arg\min_{\mathbf{x}\geq 0}\left\|\begin{pmatrix}\mathbf{A}\\ \lambda\,\mathbf{D}_{\text{aug}}\end{pmatrix}\mathbf{x} - \begin{pmatrix}\mathbf{U}\\ \mathbf{0}\end{pmatrix}\right\|_2^2. \tag{25}$$

This approach leverages established NNLS algorithms (e.g., the Lawson–Hanson method) that are described in many numerical analysis texts [25].

It should be noted that negative resistance–like contributions can occur in electrochemical impedance spectra for certain systems and operating conditions. Such observations do not imply the existence of materials with intrinsically negative resistance, but rather reflect system-level effects, for example due to inductive behavior, feedback mechanisms, variations in system parameters during measurement, or other non-RC phenomena [26,27]. Within the present framework, these effects are not explicitly represented, and negative contributions in the DRT would therefore not be physically meaningful.

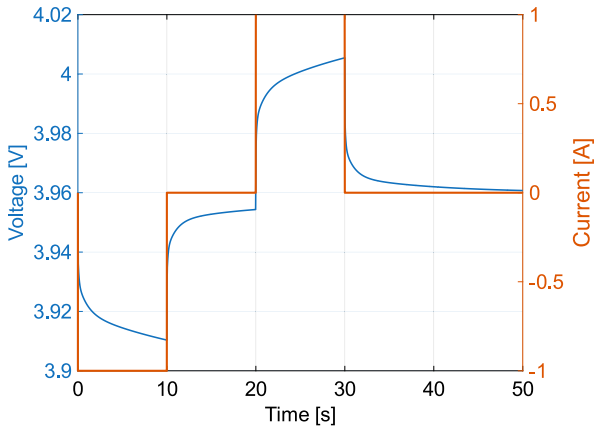

Fig. 1. Simulated current excitation and corresponding voltage response.

Furthermore, inductive behavior cannot be described by the current formulation of the model. The implications of this limitation are acknowledged, and the analysis presented here is intentionally restricted to systems for which a passive RC-based representation is appropriate.

3. Results

This section presents the results obtained from both simulated and experimental evaluations of the proposed identification algorithm. First, a synthetic cell model was used to assess the algorithm's performance under controlled and noise-affected conditions, allowing for a direct comparison between estimated and true system parameters. Subsequently, a hyperparameter analysis is conducted based on simulations with a broader relaxation time distribution. Finally, the method is applied to real world measurement data from a commercial lithium ion cell, allowing validation under practical operating conditions for different excitation strengths. In both cases, the algorithm's ability to accurately reconstruct the distribution of relaxation times and derive the corresponding impedance spectra is demonstrated.

3.1. Simulation

To evaluate the performance of the proposed method under controlled conditions, a synthetic cell was simulated. The system consists of a voltage source with a linear open-circuit voltage (OCV) characteristic corresponding to an effective differential capacitance of 3000 F. In series, four parallel RC elements were connected with time constants of 0.01 s, 0.1 s, 1 s, and 10 s, each having a resistance of 10 mΩ. Additionally, a series ohmic resistance of 10 mΩ was included.

As first excitation signal, a current profile was applied consisting of a discharge pulse of 1 A for 10 s, followed by a rest period of 10 s, a charge pulse of equal amplitude for another 10 s, and a final relaxation phase of 20 s. The signals were sampled with a temporal resolution of 1×10^{-4} s. In order to gain clearer insights into the algorithm's performance and the interpretation of the resulting residuals, no noise is added to the time series. For the DRT estimation, the time constant vector is constructed using 100 logarithmically spaced points between 1×10^{-3} s and 1×10^{2} s. Additionally, the exact time constants used in the model are explicitly included, as the automatically generated vector of logarithmically spaced time constants does not necessarily contain these exact values.

The applied current and the simulated voltage response are visualized in Fig. 1. The simulated data were subsequently analyzed using the proposed identification algorithm. The reconstructed DRT is shown in Fig. 2(a).

The estimated resistance values of the RC elements are summarized in Table 1. For this purpose, the integral over each identified peak in the DRT was calculated. The residuals between the simulated voltage response and the response of the estimated DRT are visualized in Fig. 2(b).

Table 1
Estimated resistance values of the RC elements obtained from the reconstructed DRT shown in Fig. 2(a), where the model time constant points were included in the estimation.

Model time constant τ [s]	Est. resistance [mΩ]
0.01	9.95
0.1	9.99
1.0	10.00
10.0	10.00

Table 2
Estimated resistance values of the RC elements obtained from the reconstructed DRT shown in Fig. 3(a), where the model time constant points were excluded in the estimation.

Model time constant τ [s]	Est. resistance [mΩ]
0.01	9.93
0.1	10.01
1	10.01
10	10.02

Table 3
Estimated resistance values of the RC elements obtained from the reconstructed DRT shown in Fig. 5.

Model time constant τ [s]	Est. resistance [mΩ]
0.01	9.94
0.1	10.01
1.0	10.01
10.0	9.98

The series resistance was estimated to be 10.1 mΩ, and the differential capacitance to be 3000 F. The obtained values show excellent agreement with the model parameters, demonstrating the efficiency of the algorithm on simulated data. Nevertheless, the residuals exhibit systematic behavior. To gain a better understanding of their nature, we ran the simulation a second time, this time without including the exact values of the time constants in the model for DRT estimation. The resulting DRT is shown in Fig. 3(a)

Since the exact model time constants were not additionally included in the estimation vector, the obtained peaks of the estimated DRT are smaller in magnitude and broader. This is because the solver now has to distribute the contribution to the response across shorter and longer time constants than the actual model time constant. However, the resistance values presented in Table 2 still show strong agreement with the underlying model. Similarly, the series resistance of 10 mΩ and the differential capacitance of 3006 F exhibit excellent conformity.

However, the systematic behavior of the residuals is now even more pronounced, as can be seen in Fig. 3(b). When the exact model time constants are included in the estimation, the residuals are localized within a short time span after the transient effects. This is due to a slight overestimation of the series resistance, resulting in a peak of positive residuals in Fig. 2(b), and an underestimation of the shortest time constant, which causes small oscillations of negative residuals after the peak. For the estimation with the exact time constants excluded, the algorithm cannot reproduce the precise time constants and therefore employs broader peaks in the DRT estimation. Consequently, the damped oscillation following the transients becomes much stronger, persists for a longer duration, and the peak directly at the transients increases in magnitude. Although the estimation of the series resistance remains accurate, this behavior is most likely caused by the slight underestimation of the shortest time constant.

To test a second excitation signal on the virtual system, a zero-mean pseudo-random current signal was applied. This signal consisted of

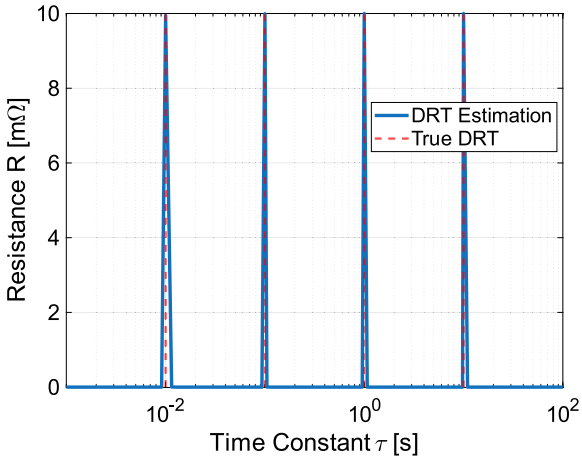

(a) Estimated DRT compared to the true time constants used in the simulation.

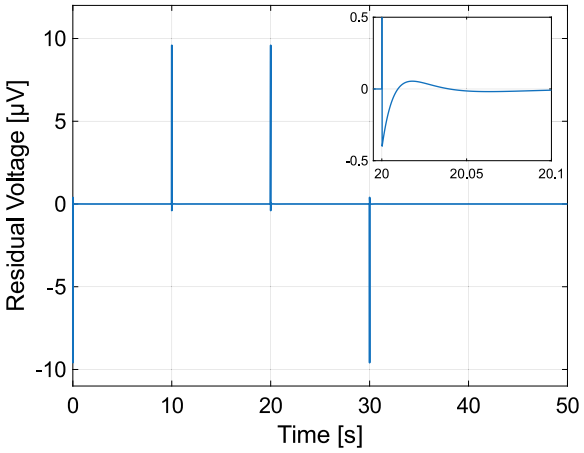

(b) Residuals between the simulated and reconstructed voltage response.

Fig. 2. DRT and residuals for estimation using time constants that do coincide with the simulated ones.

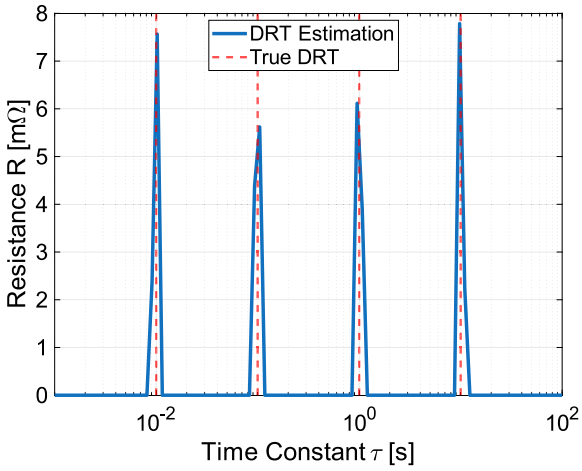

(a) Estimated DRT compared to the true time constants used in the simulation.

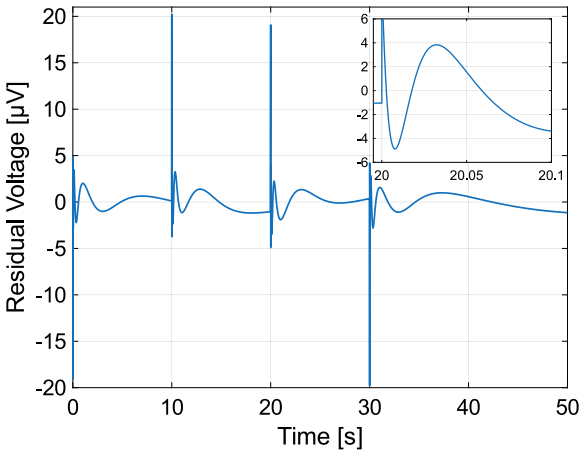

(b) Residuals between the simulated and reconstructed voltage response.

Fig. 3. DRT and residuals for estimation using time constants that do not coincide with the simulated ones.

constant-current charge and discharge steps with alternating amplitude and duration. Random noise with an amplitude of 1 mV and 1 mA was again added to both voltage and current. The sampling rate was dynamically adapted, analogous to the measurement described in Section 3.3. The applied current profile and the corresponding voltage response are illustrated in Fig. 4, along with the corresponding residuals. The estimated DRT is presented in Fig. 5. Exact model time constants are excluded from the estimation.

Once again, the algorithm demonstrates excellent performance in estimating the DRT of the system, delivering the resistance values shown in Table 3. The series resistance is accurately recovered as 10 mΩ, and the differential capacitance is estimated as 2994 F. The residuals do not exhibit any signs of systematic behavior, even without the exact time constants in the estimation, due to the much larger impact of the added noise.

The results demonstrate that the proposed method can accurately recover the underlying system parameters when the observed dynamics correspond to the assumed model structure. This confirms the numerical stability and precision of the algorithm under idealized, noise-affected conditions.

3.2. Hyperparameter analysis

In the previous section, it was demonstrated that the proposed algorithm is capable of extracting the DRT of systems composed of discrete RC elements. In real systems, such as electrochemical energy storage devices, the underlying relaxation behavior is typically characterized by a continuous distribution of time constants rather than isolated delta-dirac-like contributions. For such distributed systems, the selection of hyperparameters — specifically the regularization parameter λ and the number N of time constants used for discretization — becomes a critical aspect of the estimation procedure. A sensitivity analysis is therefore conducted to investigate the influence of these parameters on the reconstruction of a distributed DRT.

For this purpose, a synthetic DRT is generated as the superposition of two log-normal distributions defined according to Eq. (26). The corresponding parameters are summarized in Table 4.

$$g_k(\tau) = \frac{A_k}{\tau\,\sigma_k\sqrt{2\pi}} \exp\left(-\frac{(\ln\tau - \ln\tau_{0,k})^2}{2\sigma_k^2}\right) \tag{26}$$

As excitation, a current step of 1 A is simulated for 30 s, followed by a relaxation period of 70 s. Additive white noise is superimposed on

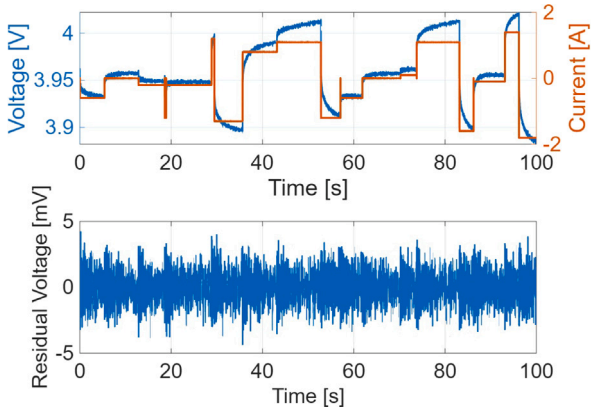

Fig. 4. Top: Simulated current excitation and corresponding voltage response for the pseudo random sequence. Bottom: residuals between the simulated and reconstructed voltage response.

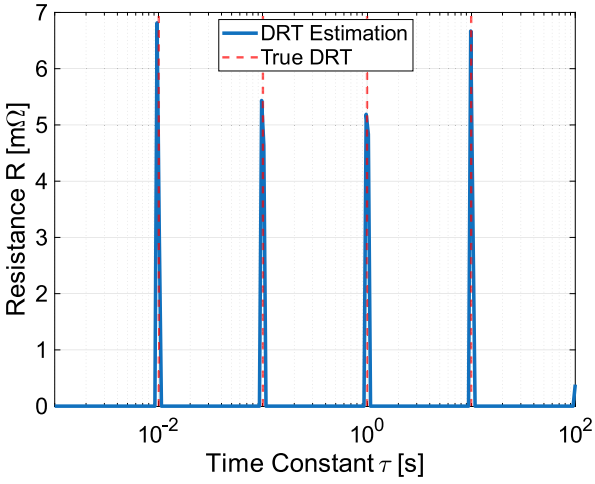

Fig. 5. Estimated DRT compared with the true time constants used in the simulation for the time series presented in Fig. 4.

Table 4
Parameters of the two log-normal distributions used to generate the synthetic DRT.

	A_k [Ω]	$\tau_{0,k}$ [s]	σ_k
g_1	0.15	0.1	0.7
g_2	150	50	0.3

both the excitation current and the voltage response with amplitudes of 0.01 A and 0.01 V, respectively. The time constant vector used for both simulation and estimation spans from 1×10^{-5} s to 1×10^{5} s.

First, the influence of the number of estimated time constants is examined. For this analysis, the algorithm is applied using different values of N, while the regularization parameter is set to zero to allow unconstrained fitting. Fig. 6 shows the resulting mean residuals as a function of N. The residuals decrease markedly with increasing N until approximately $N = 100$, beyond which further reductions become marginal while the computational cost continues to increase. An effective compromise between accuracy and computational effort is therefore achieved with approximately ten time constants per decade.

Next, the influence of the regularization parameter λ is investigated. This parameter directly controls the balance between data fidelity and smoothness of the estimated relaxation spectrum. For very small values of λ, the solution tends to overfit the noisy data, resulting in spurious or highly localized peaks in the estimated DRT. Conversely, excessively

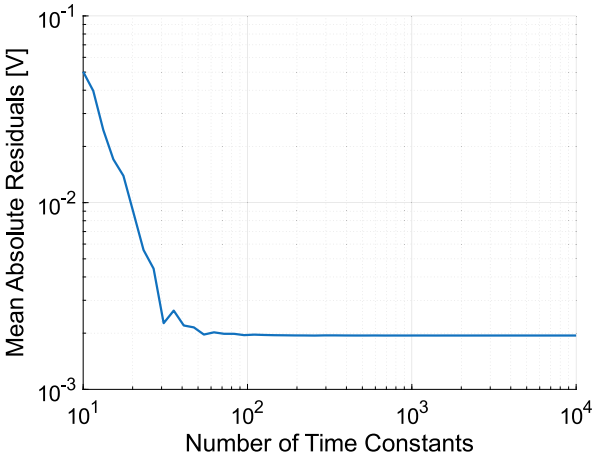

Fig. 6. Median residuals as a function of the number of estimated time constants N for zero regularization.

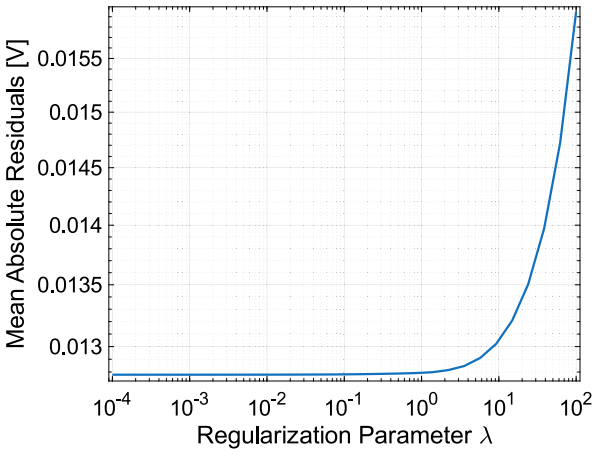

Fig. 7. Mean residuals in the time domain as a function of the regularization parameter λ.

large values of λ lead to overly smoothed solutions, potentially suppressing physically meaningful features. Such behavior is characteristic of ill-posed inverse problems.

For the following analysis, the number of time constants is fixed to $N = 200$. Fig. 7 shows the mean residuals as a function of the regularization parameter. As expected, a reduction of λ leads to decreasing residuals in the time domain. However, this trend alone is not sufficient to determine an appropriate value of λ, as very small regularization parameters result in overfitting without necessarily improving the physical interpretability of the solution. A pragmatic choice is therefore obtained by selecting the value beyond which further reductions in the residuals become negligible. For the present case, this criterion yields $\lambda = 1$.

Fig. 8 illustrates the estimated DRTs obtained for three representative values of the regularization parameter. While none of the reconstructions exactly reproduces the simulated distribution, this behavior is expected, particularly when the underlying peaks differ significantly in width. Regularization influences both the peak shapes and their amplitudes, leading to deviations from the original DRT even in cases where the time-domain residuals are comparable. This observation highlights that similar time-domain fits with equally small residuals can correspond to substantially different DRTs.

For practical interpretation, the primary quantities of interest are therefore not the exact shapes of the estimated peaks, but the characteristic time constants of the dominant processes and their contributions

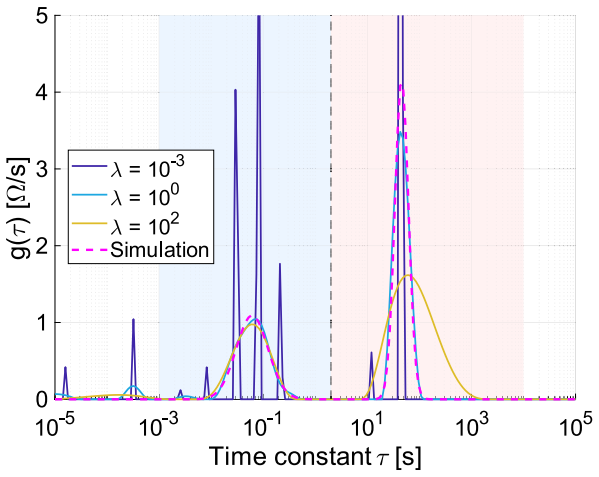

Fig. 8. Estimated DRTs for different values of the regularization parameter λ. The regions used for the integration of the resistance are indicated by shaded areas.

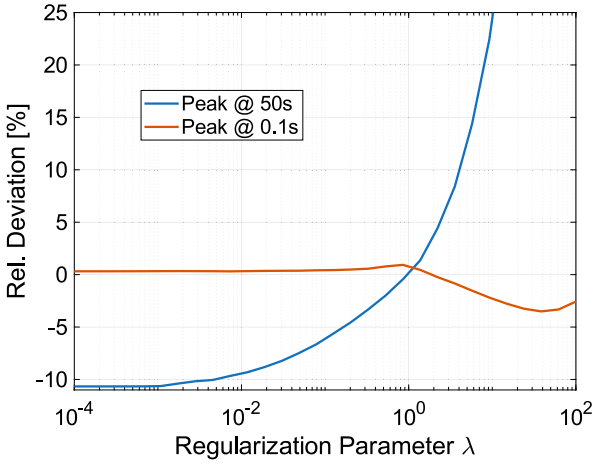

Fig. 9. Deviation of the integrated peak resistances from the simulated values as a function of the regularization parameter λ.

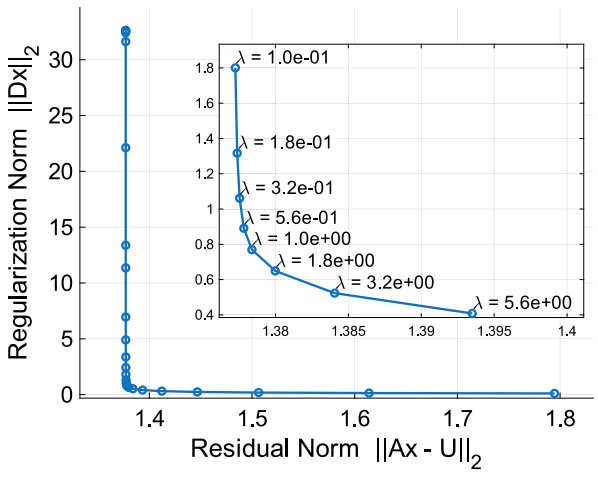

Fig. 10. L-curve analysis illustrating the trade-off between solution smoothness and residual norm for different values of λ.

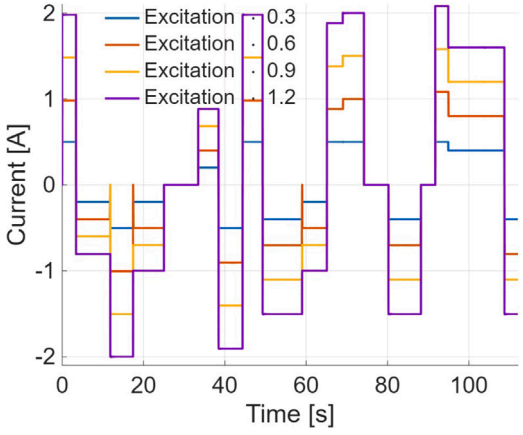

Fig. 11. Applied zero-mean pseudo-random current excitation with varying amplitude.

to the total resistance. These resistance contributions are obtained by integrating the estimated DRT over the corresponding time constant ranges. The deviation of the resulting resistance values from the simulated ones is shown in Fig. 9, indicating that the selected regularization parameter provides a reasonable compromise between accuracy and interpretability.

Furthermore, additional insights can be gained from this plot. The peak associated with short relaxation times shows only minor deviations over the investigated range of regularization parameters. This can be explained by the fact that fast relaxation processes strongly affect the early transient response and are therefore well observable in the time domain. In contrast, the resistance contribution of the peak at larger time constants depends much more strongly on the regularization strength. With increasing regularization, the smoothness constraint broadens the peak, which leads to an increase of the integrated resistance. For very small regularization parameters, the solver represents the slow process by a narrow peak close to the nominal time constant, which is sufficient to reduce the time-domain residuals but results in an underestimated resistance contribution, indicating overfitting. Overall, this analysis shows that very different relaxation spectra, both in shape and in resistance contribution, can produce nearly identical time-domain residuals, highlighting the non-uniqueness of the underlying inverse problem.

A commonly used strategy for selecting an appropriate regularization parameter is the L-curve method [24], which evaluates the trade-off between solution smoothness and residual norm. The application of this criterion to the present example is shown in Fig. 10. The point of maximum curvature is located at approximately $\lambda = 1$, in good agreement with the value obtained from the residual-based analysis.

It should be noted that the hyperparameter selection strategies discussed in this section are problem-dependent and may not be optimal in all scenarios. Their applicability should therefore be carefully assessed for each specific system and measurement configuration. Robust methods for identifying the optimal regularization parameter for time-domain estimation still need to be established.

3.3. Measurement

To validate the proposed algorithm under real-world conditions, a Samsung INR18650-30Q NMC cell with a nominal capacity of 3 Ah was used. All measurements were conducted in a climate chamber maintained at a constant temperature of 25 °C.

As excitation, a zero-mean pseudo-random current signal was applied, consisting of constant-current charge and discharge steps with alternating amplitude and duration. To investigate the influence of excitation strength on the estimation results, the same current profile was applied with different amplitude scaling factors, while preserving

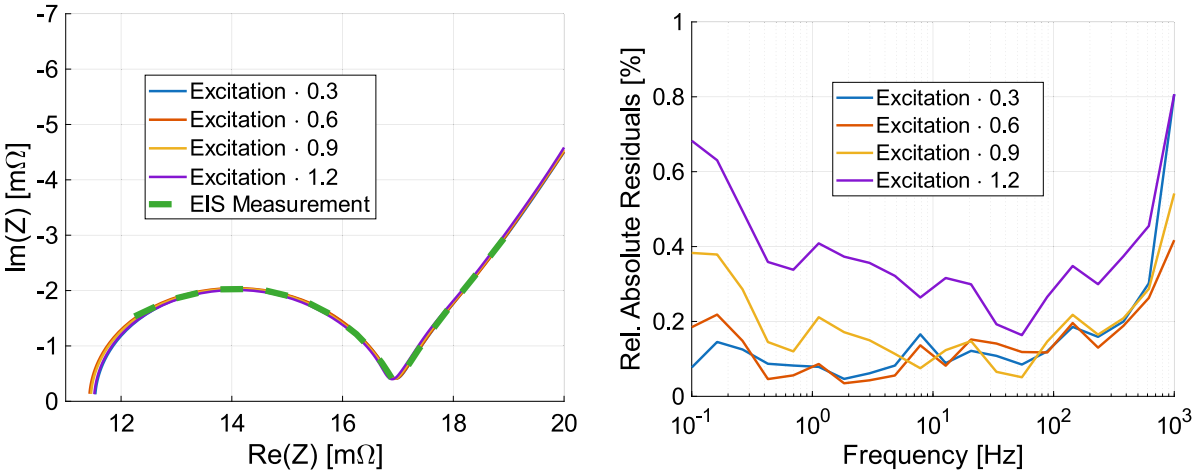

(a) Nyquist plot of measured EIS and from DRT reconstructed impedance for $\lambda = 1$.

(b) Deviation between measured EIS data and reconstructed impedance for $\lambda = 1$.

Fig. 12. EIS analysis and reconstruction accuracy.

its temporal structure. The resulting current profiles are illustrated in Fig. 11.

The current excitation and voltage response were recorded using a BatteryDynamics HRT-M battery cycler with a voltage resolution of 1 μV, configured in a four-wire setup to separate power and sense connections. The sampling rate was dynamically adapted to capture both fast transients and slow relaxation behavior. During current step transitions, a maximum sampling interval of 256 μs was applied. Subsequently, the effective sampling rate was progressively reduced by averaging consecutive measurements over increasing window sizes, preserving transient resolution while efficiently capturing long-term relaxation phenomena.

To assess the accuracy of the proposed estimation method, the estimated DRT was converted into the corresponding impedance spectrum and compared to an EIS measurement conducted immediately prior to the time-domain experiments. The EIS measurement was performed using a HIOKI BT4560 impedance spectrometer over a frequency range from 0.1 Hz to 1 kHz. The obtained EIS spectra is visualized in Fig. 12(a) and the residuals between the reconstructed and measured impedance spectra are shown in Fig. 12(b). The comparison was performed using the absolute values of the complex impedance in order to reduce the influence of phase uncertainties and to focus on deviations in the overall impedance magnitude.

For the investigated cell, the algorithm reliably captures the dominant relaxation processes and their relative contributions. A clear trend can be observed in which the deviation from the EIS measurement increases with higher excitation amplitudes. This behavior is expected, as larger current amplitudes enhance nonlinear effects that are not explicitly captured by the present linear framework [28,29]. Nevertheless, the measured and reconstructed impedance spectra show good overall agreement even at elevated excitation amplitudes, especially in the mid frequency region.

Fig. 13 shows the residuals of the estimated DRT when compared to the measured EIS spectrum as a function of the regularization parameter. For low regularization strengths, the residuals remain nearly constant and show only a weak dependence on the value of λ. Once the regularization parameter exceeds a certain threshold, which in the present case is above $\lambda = 1$, the residuals start to increase noticeably.

This behavior is consistent with the observations in the time domain and indicates that excessive regularization leads to a degradation of the impedance reconstruction. The increase in the residuals is attributed to an over-smoothing of the DRT, resulting in excessively broadened relaxation peaks and a loss of spectral resolution.

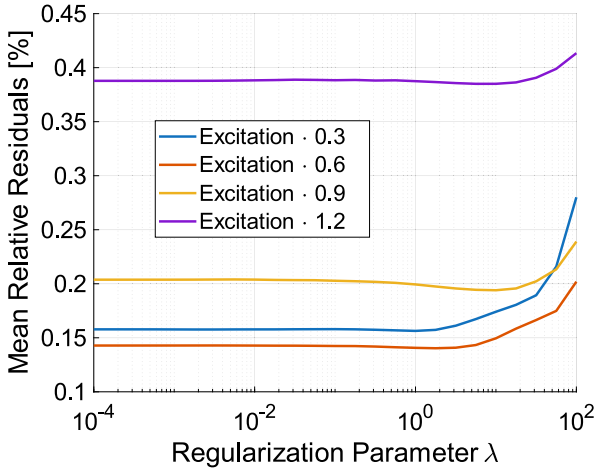

Fig. 13. Mean deviation between measured and reconstructed impedance magnitude as a function of the regularization parameter λ.

As a second benchmark, the time-domain voltage response reconstructed from the estimated DRTs is compared to the measured signal, as shown in Fig. 14. The residuals remain well below the millivolt range for all excitation amplitudes, indicating an accurate reproduction of the overall system dynamics. At the same time, the residuals exhibit clear systematic structures rather than purely random noise.

Two characteristic regions can be distinguished. The first occurs during the applied current pulses themselves and becomes more pronounced with increasing excitation amplitude, marked with an arrow. This behavior can be attributed to nonlinear effects that are not captured by the employed linear framework. Electrochemical systems may exhibit asymmetric behavior during charge and discharge, for example due to differences in charge-transfer resistance [30]. In such cases, a single linear model necessarily represents a compromise, which leads to structured residuals. Furthermore, process-related resistances may depend on the applied current amplitude, and heat generation during stronger excitation can slightly alter the internal temperature, thereby violating the assumption of time-invariant system behavior [31].

The second systematic pattern appears during rapid current changes, where short peaks appear in the residuals. As discussed in Section 3.1, these deviations can be caused by small estimation errors at very short time constants and in the series resistance.

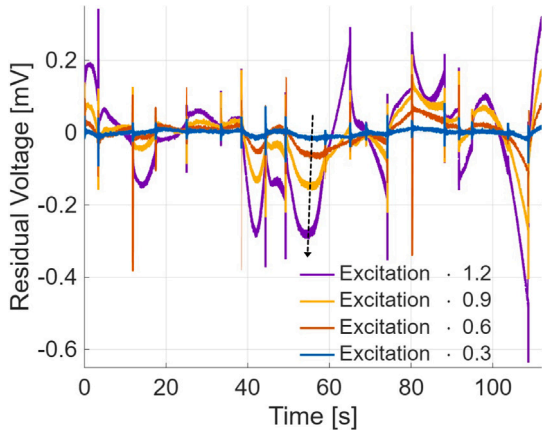

Fig. 14. Residuals between the reconstructed time-domain voltage response and the experimentally measured signal for $\lambda = 1$.

4. Conclusion and outlook

In this work, a time-domain approach for estimating the Distribution of Relaxation Times based on a recursive RC modeling framework was presented. The method enables direct DRT reconstruction from current and voltage signals without relying on frequency-domain impedance data, thereby significantly reducing measurement time, while maintaining high accuracy. The algorithm supports arbitrary excitation profiles, provided that the input signal exhibits sufficient dynamic content.

Experimental validation under controlled laboratory conditions demonstrated excellent agreement with reference electrochemical impedance spectroscopy, confirming the method's ability to identify dominant relaxation processes and their associated time constants. The recursive formulation, combined with nonnegative least squares and regularization, ensures numerical stability and physical interpretability.

The hyperparameter analysis demonstrated that the choice of the regularization parameter is crucial for obtaining a physically meaningful DRT representation. While different regularization strengths, and thus significantly different DRTs, can reproduce the time-domain dynamics with comparable accuracy, the resulting DRTs may differ substantially, in particular with respect to the resistance contributions of the underlying relaxation processes.

In real battery cells, relaxation processes form a continuous spectrum, whereas the numerical estimation relies on a discrete set of time constants. In addition, a finite sampling rate can limit the separation of very fast dynamics from the ohmic resistance, especially when the sampling frequency is not sufficiently higher than the fastest processes present. Furthermore, nonlinear effects such as current-dependent or direction-dependent resistances may contribute to the transient residuals observed in the time domain.

Despite the systematic structure of these residuals, their magnitudes remain very small, and the overall accuracy of the system identification remains high, even for increased excitation amplitudes. Nevertheless, a more detailed investigation of these effects would be beneficial and is left for future work.

In addition, future work should focus on systematically investigating the limitations of the proposed method under non-stationary and nonlinear operating conditions, such as dynamic charge/discharge cycles, temperature variations, and state-of-charge drift. These factors may violate the assumptions of linearity and time invariance, which are fundamental to the current model formulation. Furthermore, the influence of excitation signal design, for example its spectral richness and amplitude distribution, on the accuracy and resolution of the estimated DRT will be examined. Additional metrics for assessing the quality of time-domain estimations, beyond residual analysis of measured and reconstructed responses, will be explored.

CRediT authorship contribution statement

Marvin Malchau: Writing – review & editing, Writing – original draft, Visualization, Validation, Methodology, Investigation, Formal analysis, Data curation, Conceptualization. **Jan Philipp Schmidt:** Supervision.

Declaration of competing interest

The authors declare that they have no known competing financial interests or personal relationships that could have appeared to influence the work reported in this paper.

Data availability

Data will be made available on request.

References

[1] Mark Orazem, Bernard Tribollet, Electrochemical Impedance Spectroscopy, Wiley-Interscience, ISBN: 978-0470041406, 2008, http://dx.doi.org/10.1002/9780470381588.

[2] Ian D. Raistrick, J. Ross Macdonald, Donald R. Franceschetti, Impedance Spectroscopy: Theory, Experiment, and Applications, John Wiley & Sons, Ltd, ISBN: 9781119381860, 2018, http://dx.doi.org/10.1002/9781119381860.ch2, URL https://onlinelibrary.wiley.com/doi/abs/10.1002/9781119381860.ch2.

[3] Christian Plank, Tom Rüther, Leonard Jahn, Maximilian Schamel, Jan Philipp Schmidt, Francesco Ciucci, Michael A. Danzer, A review on the distribution of relaxation times analysis: A powerful tool for process identification of electrochemical systems, J. Power Sources 594 (2024) 233845, http://dx.doi.org/10.1016/j.jpowsour.2023.233845, ISSN: 0378-7753URL https://www.sciencedirect.com/science/article/pii/S0378775323012211.

[4] A.N. Tikhonov, Solution of incorrectly formulated problems and the regularization method, Sov. Math. Dokl. 4 (1963) 1035–1038.

[5] Jan Philipp Schmidt, Ellen Ivers-Tiffée, Pulse-fitting – a novel method for the evaluation of pulse measurements, demonstrated for the low frequency behavior of lithium-ion cells, J. Power Sources 315 (2016) 316–323, http://dx.doi.org/10.1016/j.jpowsour.2016.03.026, ISSN: 0378-7753, URL https://www.sciencedirect.com/science/article/pii/S0378775316302270.

[6] Erik Goldammer, Julia Kowal, Determination of the distribution of relaxation times by means of pulse evaluation for offline and online diagnosis of lithium-ion batteries, Batteries 7 (2) (2021) http://dx.doi.org/10.3390/batteries7020036, ISSN: 2313-0105, URL https://www.mdpi.com/2313-0105/7/2/36.

[7] Alexander Karger, Leo Wildfeuer, Arpit Maheshwari, Nikolaos Wassiliadis, Markus Lienkamp, Novel method for the on-line estimation of low-frequency impedance of lithium-ion batteries, J. Energy Storage 32 (2020) 101818, http://dx.doi.org/10.1016/j.est.2020.101818, ISSN: 2352-152X, URL https://www.sciencedirect.com/science/article/pii/S2352152X20316558.

[8] D. Klotz, M. Schönleber, J.P. Schmidt, E. Ivers-Tiffée, New approach for the calculation of impedance spectra out of time domain data, Electrochim. Acta 56 (24) (2011) 8763–8769, http://dx.doi.org/10.1016/j.electacta.2011.07.096, ISSN: URL https://www.sciencedirect.com/science/article/pii/S001346861101142X.

[9] Kazuo Onda, Masato Nakayama, Kenichi Fukuda, Kenji Wakahara, Takuto Araki, Cell impedance measurement by Laplace transformation of charge or discharge current–Voltage, J. Electrochem. Soc. 153 (6) (2006) A1012, http://dx.doi.org/10.1149/1.2189268.

[10] Masayuki Itagaki, Masaki Ueno, Yoshinao Hoshi, Isao Shitanda, Simultaneous determination of electrochemical impedance of lithium-ion rechargeable batteries with measurement of charge-discharge curves by wavelet transformation, Electrochim. Acta 235 (2017) 384–389, http://dx.doi.org/10.1016/j.electacta.2017.03.077, ISSN: 0013-4686, URL https://www.sciencedirect.com/science/article/pii/S001346861730542X.

[11] Manuel Kasper, Manuel Moertelmaier, Hartmut Popp, Ferry Kienberger, Nawfal Al-Zubaidi R-Smith, Reconstruction of electrochemical impedance spectroscopy from time-domain pulses of a 3.7 kWh lithium-ion battery module, Electrochem 6 (2) (2025) http://dx.doi.org/10.3390/electrochem6020017, ISSN: 2673-3293, URL https://www.mdpi.com/2673-3293/6/2/17.

[12] Leo Wildfeuer, Philipp Gieler, Alexander Karger, Combining the distribution of relaxation times from EIS and time-domain data for parameterizing equivalent circuit models of lithium-ion batteries, Batteries 7 (3) (2021) http://dx.doi.org/10.3390/batteries7030052, ISSN: 2313-0105, URL https://www.mdpi.com/2313-0105/7/3/52.

[13] Rui Xiong, Jiayi Cao, Quanqing Yu, Hongwen He, Fengchun Sun, Critical review on the battery state of charge estimation methods for electric vehicles, IEEE Access 6 (2018) 1832–1843, http://dx.doi.org/10.1109/ACCESS.2017.2780258.

[14] Tom Rüther, Maximilian Schamel, Christian Plank, Felix Schomburg, Fridolin Röder, Michael A. Danzer, Cell-to-cell variation beyond parameter analysis — identification and correlation of processes in lithium-ion batteries using a combined distribution of relaxation times analysis, J. Power Sources 587 (2023) 233677, http://dx.doi.org/10.1016/j.jpowsour.2023.233677, ISSN: 0378-7753, URL https://www.sciencedirect.com/science/article/pii/S0378775323010534.

[15] Muhammad Sohaib, Woojin Choi, Evaluating the status of lithium-ion cells without historical data using the distribution of relaxation time method, Batteries 11 (10) (2025) http://dx.doi.org/10.3390/batteries11100366, ISSN: 2313-0105, URL https://www.mdpi.com/2313-0105/11/10/366.

[16] Muhammad Sohaib, Abdul Shakoor Akram, Woojin Choi, Analysis of aging and degradation in lithium batteries using distribution of relaxation time, Batteries 11 (1) (2025) http://dx.doi.org/10.3390/batteries11010034, ISSN: 2313-0105, URL https://www.mdpi.com/2313-0105/11/1/34.

[17] Pietro Iurilli, Claudio Brivio, Vanessa Wood, Detection of lithium-ion cells' degradation through deconvolution of electrochemical impedance spectroscopy with distribution of relaxation time, Energy Technol. 10 (10) (2022) 2200547, http://dx.doi.org/10.1002/ente.202200547, URL https://onlinelibrary.wiley.com/doi/abs/10.1002/ente.202200547.

[18] Guillaume Thenaisie, Claudio Brivio, Hystimator: DRT-based hysteresis modelling for accurate SoC estimation in LFP battery cells, IET Renew. Power Gener. 18 (S1) (2024) 4387–4398, http://dx.doi.org/10.1049/rpg2.13130, URL https://ietresearch.onlinelibrary.wiley.com/doi/abs/10.1049/rpg2.13130.

[19] Alan Oppenheim, Ronald Schafer, Discrete-Time Signal Processing, Pearson Deutschland, ISBN: 9781292025728, 2013, p. 1056, URL https://elibrary.pearson.de/book/99.150005/9781292038155.

[20] John Proakis, Dimitris Manolakis, Digital signal processing: Principles, algorithms, and applications, Pearson Deutschland, ISBN: 978-1292025735, 2013, URL https://elibrary.pearson.de/book/99.150005/9781292038162.

[21] William H. Press, Saul A. Teukolsky, William T. Vetterling, Brian P. Flannery, Numerical Recipes 3rd Edition: The Art of Scientific Computing, third ed., Cambridge University Press, USA, ISBN: 0521880688, 2007.

[22] Per Christian Hansen, Discrete Inverse Problems, Society for Industrial and Applied Mathematics, 2010, http://dx.doi.org/10.1137/1.9780898718836, URL https://epubs.siam.org/doi/abs/10.1137/1.9780898718836.

[23] Lloyd N. Trefethen, David Bau III, Numerical linear algebra, Society for Industrial and Applied Mathematics, Philadelphia, PA, 1997, http://dx.doi.org/10.1137/1.9780898719574, URL https://epubs.siam.org/doi/abs/10.1137/1.9780898719574.

[24] Heinz W. Engl, Wilhelm Grever, Using the L-curve for determining optimal regularization parameters, Numer. Math. 69 (1994) 25–31, http://dx.doi.org/10.1007/s002110050078.

[25] Charles L. Lawson, Richard J. Hanson, Solving Least Squares Problems, Society for Industrial and Applied Mathematics, 1995, http://dx.doi.org/10.1137/1.9781611971217, URL https://epubs.siam.org/doi/abs/10.1137/1.9781611971217.

[26] Dino Klotz, Negative capacitance or inductive loop? – a general assessment of a common low frequency impedance feature, Electrochem. Commun. 98 (2019) 58–62, http://dx.doi.org/10.1016/j.elecom.2018.11.017, ISSN: 1388-2481, URL https://www.sciencedirect.com/science/article/pii/S1388248118303084.

[27] Tobias Franz, Tamara Miličić, Georgios Papakonstantinou, Tanja Vidaković-Koch, Kai Sundmacher, On the origin of low-frequency inductive loops in the impedance spectra of proton exchange membrane water electrolyzers, J. Power Sources 655 (2025) 237981, http://dx.doi.org/10.1016/j.jpowsour.2025.237981, ISSN: 0378-7753, URL https://www.sciencedirect.com/science/article/pii/S0378775325018178.

[28] Matthew D. Murbach, Victor W. Hu, Daniel T. Schwartz, Nonlinear electrochemical impedance spectroscopy of lithium-ion batteries: Experimental approach, analysis, and initial findings, J. Electrochem. Soc. 165 (11) (2018) A2758, http://dx.doi.org/10.1149/2.0711811jes.

[29] Nina Harting, Nicolas Wolff, Fridolin Röder, Ulrike Krewer, Nonlinear frequency response analysis (NFRA) of lithium-ion batteries, Electrochim. Acta 248 (2017) 133–139, http://dx.doi.org/10.1016/j.electacta.2017.04.037, ISSN: 0013-4686, URL https://www.sciencedirect.com/science/article/pii/S0013468617307934.

[30] Jun Huang, Hao Ge, Zhe Li, Jianbo Zhang, Dynamic electrochemical impedance spectroscopy of a three-electrode lithium-ion battery during pulse charge and discharge, Electrochim. Acta 176 (2015) 311–320, http://dx.doi.org/10.1016/j.electacta.2015.07.017, ISSN: 0013-4686, URL https://www.sciencedirect.com/science/article/pii/S0013468615300852.

[31] Toshiyuki Ohashi, Takeshi Abe, Toshiharu Fukunaga, Zempachi Ogumi, Eiichiro Matsubara, Analysis of cathode reactions of lithium ion cells using dynamic electrochemical impedance, J. Electrochem. Soc. 167 (2) (2020) 020502, http://dx.doi.org/10.1149/1945-7111/ab6281.